ACS APPLIED MATERIALS & INTERFACES

Forum Article

www.acsami.org

Influence of Luminescence Quantum Yield, Surface Coating, and Functionalization of Quantum Dots on the Sensitivity of Time-Resolved FRET Bioassays

K. David Wegner,[†] Phung Thi Lanh,[†] Travis Jennings,[‡] Eunkeu Oh,[§,⊥] Vaibhav Jain,[§] Simon M. Fairclough,[#] Jason M. Smith,[#] Emerson Giovanelli,[∥] Nicolas Lequeux,[∥] Thomas Pons,[∥] and Niko Hildebrandt[†,*]

[†]Institut d'Electronique Fondamentale, Université Paris-Sud, 91405 Orsay Cedex, France

[‡]eBioscience, Inc., 10255 Science Center Drive San Diego, California 92121, United States

[§]Optical Sciences Division, Code 5600, U.S. Naval Research Laboratory, Washington, D.C. 20375, United States

[⊥]Sotera Defense Solutions, Annapolis Junction, Maryland 20701, United States

[#]Department of Materials, University of Oxford, Oxford, Oxfordshire, OX1 3PH, United Kingdom

[∥]Laboratoire de Physique et d'Etude des Matériaux, ESPCI-CNRS-UPMC UMR8213, 75005 Paris, France

Supporting Information

ABSTRACT: In clinical diagnostics, homogeneous time-resolved (TR) FRET immunoassays are used for fast and highly sensitive detection of biomarkers in serum samples. The most common immunoassay format is based on europium chelate or cryptate donors and allophycocyanin acceptors. Replacing europium donors with terbium complexes and the acceptors with QDs offers large photophysical advantages for multiplexed diagnostics, because the Tb-complex can be used as FRET donor for QD acceptors of different colors. Water-soluble and biocompatible QDs are commercially available or can be synthesized in the laboratory using many available recipes from the literature. Apart from the semiconductor material composition, an important aspect of choosing the right QD for TR-FRET assays is the thickness of the QD coating, which will influence the photophysical properties and long-term stability as well as the donor−acceptor distance and FRET efficiency. Here we present a detailed time-resolved spectroscopic study of three different QDs with an emission maximum around 605 nm for their application as FRET acceptors (using a common Tb donor) in TR-bioassays: (i) Invitrogen/Life Technologies Qdot605, (ii) eBioscience eFluorNC605 and iii) ter-polymer stabilized CdSe/CdS/ZnS QDs synthesized in our laboratories. All FRET systems are very stable and possess large Förster distances (7.4−9.1 nm), high FRET efficiencies (0.63−0.80) and low detection limits (0.06−2.0 pM) within the FRET-bioassays. Shapes, sizes and the biotin/QD ratio of the biocompatible QDs could be determined directly in the solution phase bioassays at subnanomolar concentrations. Both commercial amphiphilic polymer/lipid encapsulated QDs and self-made ligand-exchanged QDs provide extremely low detection limits for highly sensitive TR-FRET bioassays.

KEYWORDS: *FRET, quantum dot, biosensor, diagnostics, terbium, multiplexing, spectroscopy, immunoassay, biotin, streptavidin*

INTRODUCTION

Semiconductor nanocrystals or quantum dots (QDs) are important fluorophores for optical biosensing applications because they combine spectrally broad absorption with high molar absorptivity and spectrally narrow emission with high brightness.[1−4] Three-dimensional quantum confinement allows tuning of absorption and emission wavelengths over a large range of the UV−vis−NIR spectral region by changing QD sizes and/or materials.[1,5] Despite the photophysical advantages of QDs, their applications in biosensing remain most often limited to research studies. The adoption of QDs within clinical diagnostic kits is still limited although several commercial suppliers of biocompatible QDs exist.[6] QDs with superior photoluminescence (PL) properties are usually synthesized in organic solvents and thus they require exchange of surface ligands or coating with water-soluble shells (e.g., polymers or lipids) in order to be used in aqueous solutions.[7,8] Such steps can cause significant alterations in brightness, stability and/or size of the QDs. Moreover, the relatively large surfaces of QDs give rise to multiple interactions with the biological environment, which can cause further changes in the physical and chemical properties of QDs. It is therefore very important to investigate various different QDs for each application. A detailed steady-state and time-resolved spectroscopic analysis

Special Issue: Forum on Biomedical Applications of Colloidal Photoluminescent Quantum Dots

Received: December 11, 2012
Accepted: February 27, 2013
Published: March 15, 2013

Scheme 1. Time-Resolved Tb-to-QD FRET Bioassay Using Tb-Labeled Streptavidin (sAv) and Biotinylated (B) QDs for Biological Recognition[a]

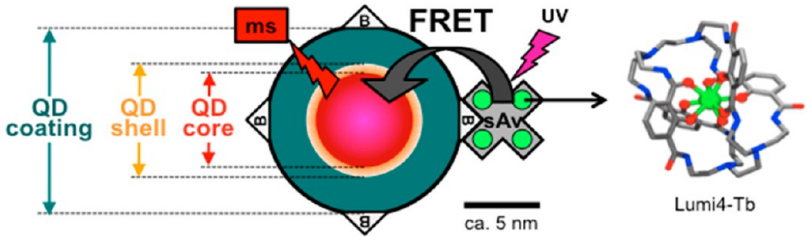

[a]Once the binding is established, the close proximity between the Tb-complexes (Lumi4-Tb) and the QD enables efficient FRET. Three different biotinylated QDs with emission maxima at ca. 605 nm were investigated: Commercial Qdot605 (Invitrogen/Life Technologies), eFluorNC605 (eBioscience), and self-made CdSe/CdS/ZnS core/shell/shell QDs. The cross shape of sAv represents the four binding sites for biotin. The four Lumi4-Tb are bound to free lysine groups of sAv and are therefore randomly distributed over the sAv. This distribution as well as the non-spherical shapes of the QDs (cf. Figure 3) lead to a Lumi4-Tb to QD-center distance distribution. Out of this distribution, we could identify three main distances that were further averaged to one average Tb-to-QD distance (cf. Table 2). Biotin and Lumi4-Tb (adapted from ref 22, copyright 2011 American Chemical Society) not to scale.

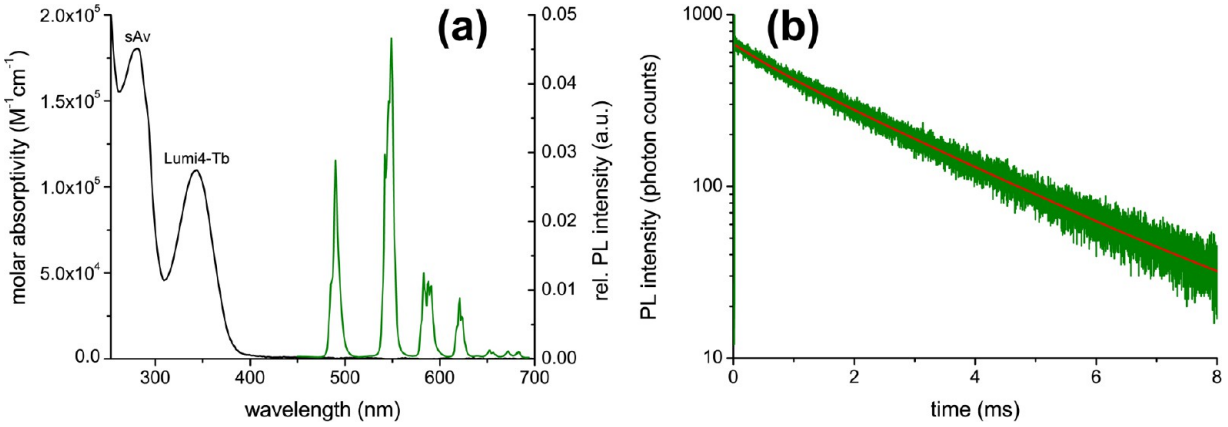

Figure 1. (a) Absorbance (black) and emission (green) spectra λ_{ex} = (350 ± 1) nm of the Lumi4-Tb-sAv donor. (b) Luminescence decay curve (green) and respective fit (red) of Lumi4-Tb-sAv leading to an amplitude-weighted average lifetime of $\langle\tau\rangle$ = 2290 μs λ_{ex} = (350 ± 1) nm, λ_{em} = (490 ± 1) nm.

using all fluorescent and biological components necessary for a sensitive bioassay can reveal much important information for bringing the QD-based biosensor a significant step closer to its integration into the "real world" of diagnostics.

Typical bioassays used in such diagnostic applications are FRET (Förster resonance energy transfer) immunoassays, for which two primary antibodies against different epitopes on the same biomarker are conjugated with a FRET donor and acceptor, respectively. FRET immunoassays are homogeneous (no washing or separation steps required), inherently ratiometric (ratio of FRET-sensitized acceptor and FRET-quenched donor fluorescence can be measured) and very sensitive (fluorescence detection), which make them especially interesting for quick and facile diagnostic tests, detecting low concentrations of biomarkers (e.g., in point-of-care diagnostics).[9] Luminescent lanthanide complexes provide another important contribution to FRET immunoassays. The long luminescence lifetimes of lanthanides offer the possibility of time-gated or time-resolved detection, which leads to a significant autofluorescence background suppression and therefore the realization of lower detection limits.[10−13] These assays are frequently used in "real world" diagnostics and are commercially available under brand names such as HTRF (homogeneous time-resolved fluorescence), TRACE (time-resolved amplified cryptate emission) or LANCE (lanthanide chelate excitation).[14−16]

In prior work we have demonstrated the benefits of combining lanthanide donors with quantum dot acceptors for different multiplexed FRET bioassay formats.[17−21] Here we present a spectroscopic investigation of one of the main materials and interfaces used within these assays, the QDs. Taking advantage of biotin-streptavidin (biot-sAv) recognition, we established a comparative study of time-resolved FRET between a commercial luminescent terbium complex (Lumi4-Tb, Lumiphore, Inc., USA) labeled to sAv and three different biotinylated CdSe-based QDs emitting around 605 nm (Scheme 1). Two batches of QDs with amphiphilic polymer/lipid coatings from commercial sources (Qdot605 from Invitrogen by LifeTechnologies Corp., USA and eFluorNC605 by eBioscience, Inc., USA), and one batch of QDs coated with poly(dithiol-co-sulfobetaine) polymeric ligands (pDTSB), synthesized in our laboratories, were compared. All tested systems showed efficient FRET, high stability in biological buffers and femto- to picomolar limits of detection (LODs). Simultaneous time-resolved (TR) luminescence detection of donor and acceptor emission allowed us to analyze the FRET processes from the energy-providing (donor) and the energy-receiving (acceptor) side. Thus we were able to measure precisely FRET efficiencies, QD sizes and shapes, and

quantification of biotin per QD ratios as well as their influence on LODs using subnanomolar concentrations and low-volume (150 μL) samples.

EXPERIMENTAL SECTION

Materials. The terbium complex conjugated to streptavidin (Lumi4-Tb-sAv) was produced and provided by Lumiphore (Richmond, USA). The CdSe/ZnS core/shell-based biotinylated QD Qdot605 was purchased from Invitrogen (Qdot605 biotin conjugate, Life Technologies, Carlsbad, USA). The CdSe/ZnS core/shell-based biotinylated QD eFluorNC605 was produced and provided by eBioscience (San Diego, USA). The CdSe/CdS/ZnS core/shell/shell-based biotinylated QDs p(DT-SB)605(A) and p(DT-SB)605(B) were synthesized using standard synthetic procedures in non-coordinating high-boiling-point solvents,[23,24] and cap exchanged with p(DT-SB) as well as biotinylation following previously described procedures.[25] Unconjugated biotins were purified using ultrafiltration and size exclusion chromatography.[25] For all measurements (unless mentioned differently) sodium-tetraborate with a pH of 8.5 was used as buffer. In case of the FRET-assay measurements bovine serum albumin (BSA, Sigma-Aldrich, Lyon, France) was added to the buffer. All chemicals were used as received. Water was purified by Purelab Option-Q (ELGA Labwater Veolia water STI, Antony, France).

Analytical Methods. Structural characterization of the Qdot605 was carried out using a JEOL 2100-FS analytical high-resolution transmission electron microscope (HR-TEM) with a 200 kV accelerating voltage. Samples for TEM were prepared by spreading a drop of the QD dispersion onto the ultrathin carbon film on holey carbon support film on Au grid (300 mesh, Ted Pella, Inc.) and letting it dry. TEM images of the eFluorNC605 were taken using a JEOL 2010 running at 200 kV. A solution diluted in chloroform was dropcast on Cu grid with ultrathin carbon support and left overnight to dry. TEM images of the homemade biotinylated p(DT-SB) QDs were acquired on a JEOL 2010F microscope operated at 200 kV. Photoluminescence quantum yields of the QDs were measured using fluorescein in basic ethanol (97%) and rhodamine 6G in ethanol (95%) as standards.[26] Absorbance measurements were performed on a SPECTROstar^{Nano} (BMG-Labtech, Germany) in combination with the LVis-microplate. The Lumi4-Tb/sAv labeling ratio was determined by the absorbance spectrum (Figure 1a) using molar absorptivities of ε(343 nm) = 26 000 M^{-1} cm^{-1} and ε(280 nm) = 2600 M^{-1} cm^{-1} for Lumi4-Tb and ε(280 nm) = 168 000 M^{-1} cm^{-1} for the tetrameric protein sAv (24 tryptophans (n_{Trp}), 24 tyrosines (n_{Tyr}), and no disulfide bonds (n_{dsb}) using the following equation:[27] $\varepsilon(280\text{ nm}) = (5500n_{Trp} + 1490n_{Tyr} + 125n_{dsb})$ M^{-1} cm^{-1}.

PL spectra and decay curves for the characterization of the samples were measured on the fluorescence spectrometer FluoTime 300 "Easy Tau" (PicoQuant, Germany). For the PL decay curve of Lumi4Tb-sAv a xenon flash lamp with a repetition rate of 100 Hz at 350 nm was used. In case of the QDs a picosecond pulsed diode laser EPL-405 (Edinburgh Instruments, UK) with a center wavelength of (405 ± 7) nm and repetition rate of 2 MHz was used. The PL decay curves were fitted with FluoFit Pro version 4.4.1.0. (PicoQuant, Germany). For the measurement of the PL decay curves of the Tb to QD FRET an EI fluorescence plate reader (Edinburgh Instruments, UK) with 4000 detection bins of 2 μs integration time was used. A nitrogen laser VSL 337 ND (Spectra Physics, USA) was used for excitation (337.1 nm, 20 Hz, 600 flashes). (494 ± 20) nm and (660 ± 13) nm bandpass filters were used for donor and acceptor, respectively. The data were fitted with FAST software version 3.1 (Edinburgh Instruments, UK). Time-gated intensity measurements for the FRET-assays were obtained with a modified KRYPTOR fluorescence plate reader (Cezanne/Thermo Fisher Scientific, France) using 500 detection bins of 2 μs integration time. An integrated nitrogen laser was used for excitation (337.1 nm, 20 Hz, 100 flashes). The same bandpass filters as within the EI plate reader were used. Time-gated PL intensities (100 to 900 μs) were acquired simultaneously for donor and acceptor. All FRET assays were measured in black 96-well microtiter plates with an optimal working volume of 150 μL. Lumi4Tb-sAv concentration was kept constant at 0.2 nM in all FRET-assay measurements. QD concentrations were varied from 0.02 nM to 0.6 nM. Each QD concentration was prepared three times. The pure Lumi4-Tb-sAv sample (zero QD concentration) was prepared ten times. All samples were measured in triplicates. In control measurements the different QD concentrations were measured without the presence of Lumi4Tb-sAv. After preparation the samples were incubated for 90 min at 37 °C before the measurements in the EI and KRYPTOR fluorescence plate readers. OriginPro 8.1 SR3 (OriginLab Corporation) and Microsoft Excel (Microsoft Corporation) were used for graphs and calculations.

PL Decay Time Analysis. The decay time analysis in the donor and acceptor channel was performed as follows for every FRET system. Due to the large difference in the excited-state lifetimes of Tb and QD (ca. 5 orders of magnitude, vide infra) the decay times caused by FRET are the same for Tb (decay time of the donor in presence of the acceptor τ_{DA}) and QD (decay time of the acceptor in the presence of the donor $\tau_{AD} = \tau_{DA}$).[18] All decay curves were fitted using a multiexponential PL intensity decay function

$$I = \sum A_i \exp(-t/\tau_i) = A \sum \alpha_i \exp(-t/\tau_i) \quad (1)$$

where A is the total amplitude and α_i are the amplitude fractions ($\Sigma\alpha_i = 1$). All PL lifetime averaging for the dynamic FRET quenching process was performed using amplitude weighted average lifetimes[28,29]

$$\langle\tau\rangle = \sum \alpha_i \tau_i \quad (2)$$

First the decay curve of the pure Lumi4-Tb-sAv donor (e.g., gray curve in Figure 4c for the eFluorNC605 FRET system) was fitted using a double-exponential decay function, which led to the amplitude fractions α_{D1} and α_{D2}, the PL decay times τ_{D1} and τ_{D2} (with $\tau_{D2} > \tau_{D1}$) and the average PL decay time of the pure donor (in the absence of the acceptor) $\langle\tau_D\rangle$. The FRET-quenched decay curves in the donor detection channel were fitted using a triple-exponential decay function, leading to the amplitude fractions α_{DA*1}, α_{DA*2}, and α_{DA*3} and the PL decay times τ_{DA1}, τ_{DA2}, and τ_{DA3}, for which the third decay time component was fixed to $\tau_{DA3} = \tau_{D2}$ in order to take into account the emission of unquenched donors. For the calculation of the average donor decay time in the presence of the acceptor $\langle\tau_{DA}\rangle$, only the first two amplitudes and decay times were used (as the third component represents unquenched donors). Therefore, the amplitude fractions must be redefined for these two decay times τ_{DA1} and τ_{DA2}

$$\alpha_{DA1} = \frac{\alpha_{DA*1}}{\alpha_{DA*1} + \alpha_{DA*2}} \text{ and } \alpha_{DA2} = \frac{\alpha_{DA*2}}{\alpha_{DA*1} + \alpha_{DA*2}} \quad (3)$$

As the unquenched donor possesses two decay time components (τ_{D1} and τ_{D2}), $\langle\tau_{DA}\rangle$ must be corrected for the shorter time component (τ_{D1}). As this shorter decay time of the "pure" donor falls within the time-range of the FRET-quenched decay times, the use of an additional exponential for the fit procedure leads to inconsistent fit results. We therefore applied a correction factor z_D (the fraction of unquenched donors in the short time components), which is determined by comparing the amplitude fractions of τ_{D2} and τ_{DA3} ($\tau_{DA3} = \tau_{D2}$) multiplied by the amplitude fraction α_{D1}

$$z_D = \alpha_{D1}(\alpha_{DA*3}/\alpha_{D2}) \quad (4)$$

The average FRET-quenched decay time is then

$$\langle\tau_{DA}\rangle = \frac{\alpha_{DA1}\tau_{DA1} + \alpha_{DA2}\tau_{DA2} - z_D\tau_{D1}}{1 - z_D} \quad (5)$$

and the average FRET-efficiency is

$$\langle\eta_{FRET}\rangle = 1 - \frac{\langle\tau_{DA}\rangle}{\langle\tau_D\rangle} \quad (6)$$

The FRET-sensitized decay curves in the acceptor detection channel were fitted using a quadruple-exponential decay function, leading to the amplitude fractions α_{AD*0}, α_{AD*1}, α_{AD*2}, and α_{AD*3} and the PL decay times τ_{AD0}, τ_{AD1}, τ_{AD2} and τ_{AD3}, for which the fourth decay time component was fixed to $\tau_{AD3} = \tau_{D2}$ in order to take into account the

emission of unquenched donors, which is much less intense compared to the donor channel but still present due to spectral crosstalk of the Tb emission in the QD acceptor detection channel. The correction factor z_A (the fraction of unquenched donors in the short time components) is almost negligible but is still taken into account for a correct treatment

$$z_A = \alpha_{D1}(\alpha_{AD*3}/\alpha_{D2}) \quad (7)$$

To calculate the average FRET decay time $\langle\tau_{AD}\rangle$ only the amplitudes and lifetimes with $i = 0-2$ are taken into account ($i = 3$ represents the unquenched donor emission). Moreover, the amplitudes α_{AD*i} must be corrected by the FRET rates $k_i = 1/\tau_{ADi} - 1/<\tau_D>$, to take into account the dependence of the excitation of the acceptors (and therefore the amplitude fractions) on the different FRET efficiencies for the different distances (corresponding to the decay times τ_{ADi}). The corrected amplitude fractions are (for $i = 0-2$)

$$\alpha_{ADi} = \frac{\alpha_{AD*i}/k_i}{\sum \alpha_{AD*i}/k_i} \quad (8)$$

The average FRET decay time is then calculated by:

$$\langle\tau_{AD}\rangle = \frac{\alpha_{AD0}\tau_{AD0} + \alpha_{AD1}\tau_{AD1} + \alpha_{AD2}\tau_{AD2} - z_A\tau_{D1}}{1 - z_A} \quad (9)$$

and the average FRET-efficiency is

$$\langle\eta_{FRET}\rangle = 1 - \frac{\langle\tau_{AD}\rangle}{\langle\tau_D\rangle} \quad (10)$$

For each FRET decay time, the donor−acceptor distance r_x can be calculated by

$$r_x = R_0\left(\frac{\tau_x}{\langle\tau_D\rangle - \tau_x}\right)^{1/6} \quad (11)$$

where τ_x represents the different lifetimes τ_{DAi}, τ_{ADi}, $\langle\tau_{DA}\rangle$, or $\langle\tau_{AD}\rangle$. The fractions of FRET-pairs found at the different distances corresponding to τ_{DAi} and τ_{ADi} are given by the amplitude fractions of these decay times.

RESULTS AND DISCUSSION

Spectroscopic Analysis of FRET Donor and Acceptors.

To establish a profound basis for this comparative FRET study using one Tb-complex as donor and different QDs (Qdot605, eFluorNC605, and p(DT-SB)605) as acceptors, we performed a spectral and time-resolved analysis of the separated FRET components. The donor within all FRET-pairs (Table 1) was the supramolecular Tb-complex Lumi4-Tb labeled to streptavidin (sAv). Lumi4-Tb consists of a chelating ligand coordinating a Tb^{3+} ion in its center. The ligand shows a strong absorption band with a maximum molar absorptivity of ca. 26 000 M^{-1} cm^{-1} at 340 nm, which shifts to ca. 343 nm when labeled to sAv. The absorbance spectrum (Figure 1a) shows a linear combination of sAv (maximum at 280 nm) and Lumi4-Tb (maximum at 343 nm) absorption, resulting in a labeling ratio of ca. 4.2 Lumi4-Tb/sAv. After ligand absorption the energy is transferred to the central Tb^{3+} ion, which then shows the typical Tb-emission lines with major peaks around 490, 545, 585, and 620 nm (and some peaks with minor intensities between 645 and 690 nm). Figure 1a shows the intensity-normalized (area under the emission spectrum from 450 to 690 nm normalized to unity) emission spectrum of Lumi4-Tb. This emission has an almost monoexponential long-lifetime luminescence decay behavior (Figure 1b) with a minor decay time of 630 μs (4% and 14% of the overall intensity and amplitude, respectively) and a major decay time of 2560 μs (96% and 86% of the overall intensity and amplitude,

Table 1. Properties of the Tb Donor and the QD Acceptors Used within the FRET Study

	material	size (nm)[e]	source	biomolecule	Φ[g]	R_0 (nm)[h]
Lumi4-Tb	supramolecular Tb-complex[a]	ca. 1.0	Lumiphore	streptavidin, ca. 4.2 Lumi4-Tb/sAv	0.67	donor for all acceptors
Qdot605	CdSe/ZnS core/shell QD coated with polymer/PEG layer[b]	core/shell: 4.0 × 9.4 complete QD: 16	Invitrogen/Life Technologies	biotin, ca. 3−4 biot/QD	0.73	9.1
eFluorNC605	CdSe/ZnS core/shell QD coated with PEG-lipid layer[c]	core/shell: 6.0 complete QD: 14	eBioscience	biotin, ca. 3−4 biot/QD	0.65	7.8
p(DT-SB)605(A)	CdSe/CdS/ZnS core/shell/shell QD coated with ter-polymer layer[d]	core/shell/shell: 6−7 complete QD: 12	ESPCI[f]	biotin, ca. 3−4 biot/QD	0.07	7.4
p(DT-SB)605(B)	CdSe/CdS/ZnS core/shell/shell QD coated with ter-polymer layer[d]	core/shell/shell: 6−7 complete QD: 12	ESPCI[f]	biotin, ca. 1 biot/QD	0.07	7.4

[a]www.lumiphore.com. [b]www.invitrogen.com. [c]www.ebioscience.com. [d]Reference 25. [e]core/shell: diameters or minimum/maximum length of ellipsoid axes as measured by TEM; complete QDs incl. coating: diameters as determined by our FRET donor−acceptor distances study; hydrodynamic diameter values provided by suppliers: 16 nm for Qdot605 (size exclusion chromatography on HPLC), 20−26 nm for eFluorNC605 (DLS) and 16−18 nm for p(DT-SB)605 (DLS). [f]cf. addresses of the authors. [g]Measured in borate buffer against fluorescein and rhodamine as standards for the QDs. Measured by $\Phi = <\tau>/\tau_{int}$ for Lumi4-Tb, with τ_{int} = 3450 μs the intrinsic lifetime of Lumi4-Tb.[17] [h]Förster distances as calculated within this study (cf. Supporting Information).

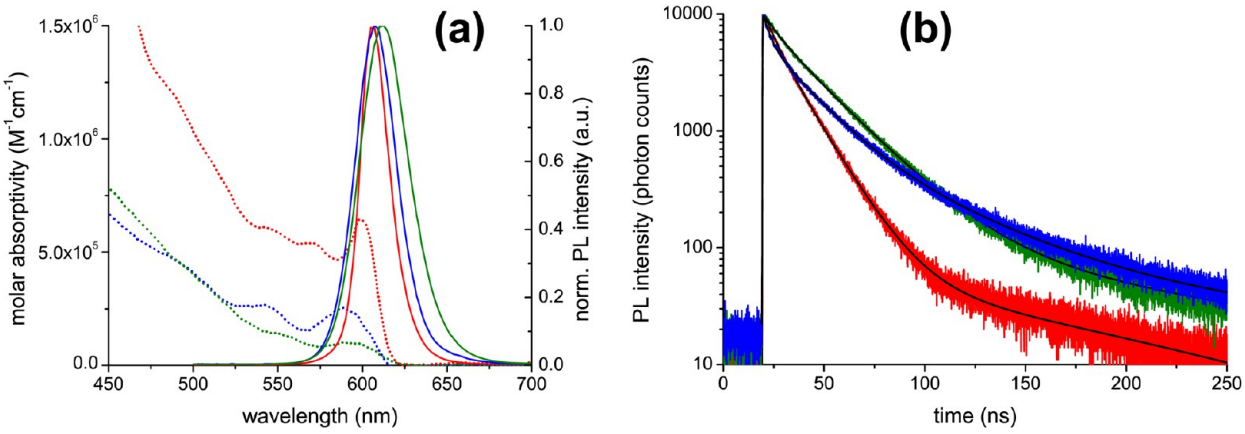

Figure 2. (a) Absorption (dotted lines) and PL emission spectra (λ_{ex} = (410 ± 0.5) nm; intensity-normalized to unity at PL maxima) of the different biotinylated QDs used as FRET acceptors. (b) PL decay curves (λ_{ex} = (405 ± 7) nm, λ_{em} in the intensity maxima) of the different biotinylated QDs and their respective multiexponential fit curves with average PL lifetimes of 17 ns (red), 29 ns (blue), and 31 ns (green). Red = Qdot605, blue = eFluorNC605, green = p(DT-SB)605.

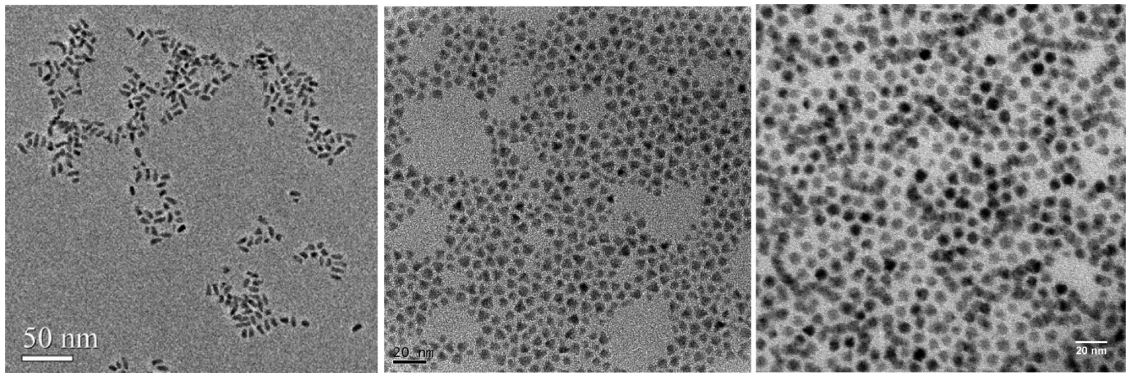

Figure 3. TEM images (showing only the core/shell structure of the QDs) of Qdot605 (left), eFluorNC605 (center), and p(DT-SB)605 (right). High-resolution images can be found in the Supporting Information, Figure S1.

respectively). The average lifetime is $\langle\tau\rangle$ = (2290 ± 100) μs. This is the amplitude-weighted average lifetime (cf. eq 2), which must be used for the donor within the dynamic FRET quenching process.[28] The long excited-state lifetime is crucial for FRET to QDs, because energy can only be transferred to the QDs after these have decayed back to their ground states following their very efficient direct excitation at the UV excitation wavelength of Lumi4-Tb. In our case the difference in lifetimes is ca. 5 orders of magnitude (ca. 2.3 ms for Lumi4-Tb and ca. 25 ns for the QDs, see Figures 1b and 2b).

The acceptors for our FRET study were different surface functionalized and biotinylated water-soluble QDs (Table 1). The p(DT-SB)605 QDs were synthesized with different amounts of biotins on the surface in order to evaluate the influence of the biotin surface coverage for biosensing applications. Apart from the Qdot605, for which a biot/QD ratio of "typically 5 to 7" is given by the supplier, all biot/QD ratios were unknown. The values in Table 1 were found within our FRET experiments (vide infra). The biot/Qdot605 ratio is 3 to 4 in our case. As a fresh sample of biot-Qdot605 was used we do not expect any loss of biotin over time. We rather assume a batch-to-batch variation as already indicated by the explanation "typically 5–7 Biotin molecules/Qdot conjugate" within the product description of LifeTechnologies. To compare the different QD performance in FRET bioassays, we chose similar absorption and emission wavelengths. As shown in Figure 2a all QDs show the characteristic broad absorption spectra with several pronounced exciton peaks between 525 and 625 nm. The absorption spectra have large molar absorptivity values and are nicely overlapping with the most intense emission peaks of Lumi4-Tb (Figure 1a), which leads to long Förster distances R_0 (the donor–acceptor distance for which FRET is 50% efficient) between 7.4 and 9.1 nm (Table 1). As the absorbance of the Qdot605 is significantly larger than for the other two QDs, it also possesses the highest R_0 in combination with Lumi4-Tb as donor. All PL spectra are very symmetrical and have a maximum intensity around 605 nm with full-width at half-maximum values of 20 nm (Qdot605), 29 nm (eFluorNC605) and 34 nm (p(DT-SB)605). The PL decay curves (Figure 2b) are multi-exponential with intensity-weighted average lifetimes of 17 ns (Qdot605), 29 ns (eFluorNC605) and 31 ns (p(DT-SB)605). Qdot605 and eFluorNC605 are very bright with PL quantum yields of 73 and 65%, respectively. p(DT-SB)605 (7%) provide significantly lower values, as expected from ligand-exchanged QDs, which are more compact but display a reduced quantum yield compared to encapsulated QDs.[30,31]

TEM images of the semiconductor parts (polymer coatings not visible) of the different QDs (Figure 3) show that the QDot605 QDs are very elongated, whereas the eFluorNC605 and p(DT-SB)605 are much closer to spherical shape, although some elongation as well as tetrahedral and star-shaped QDs are visible. The difference in shape is quite interesting because it should also become visible in the FRET data due to the

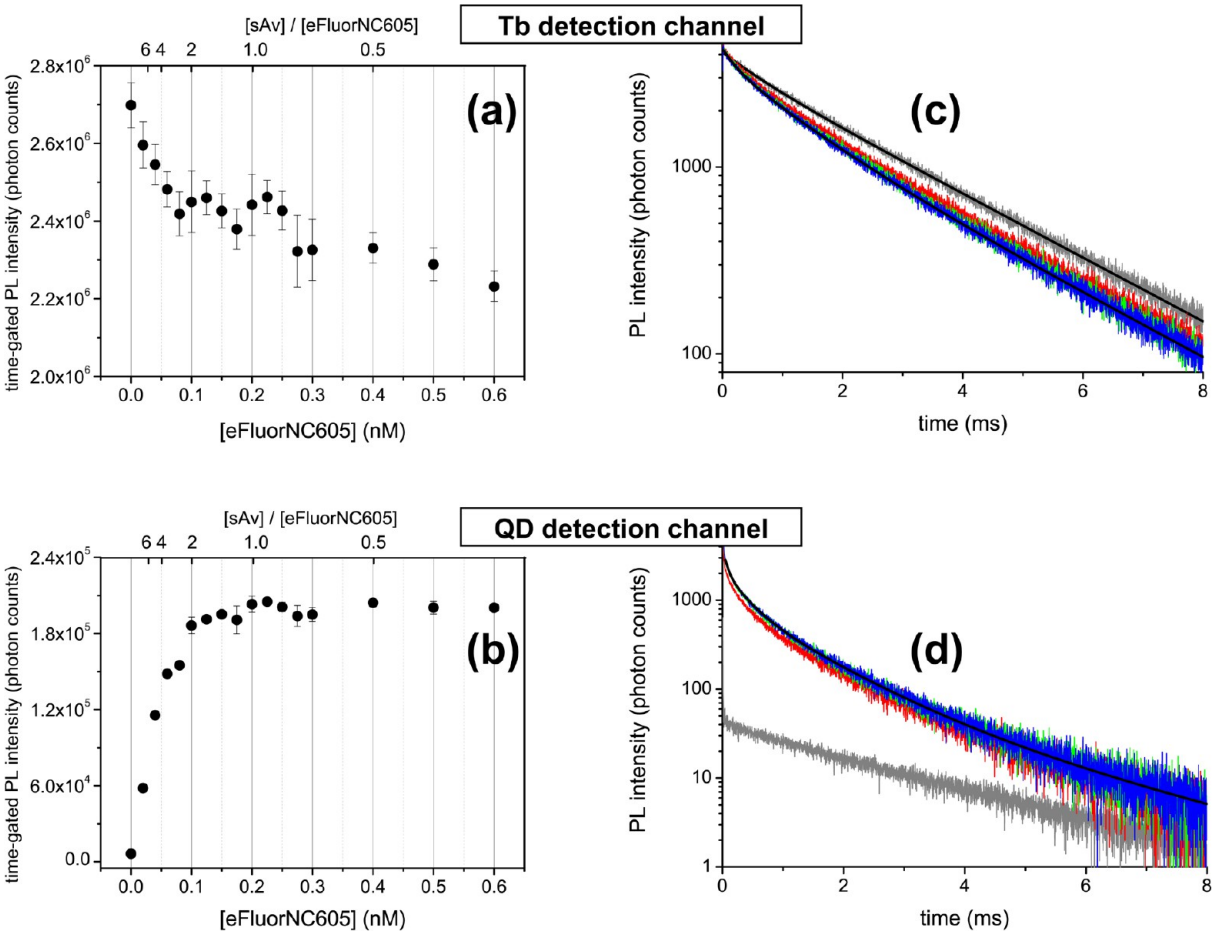

Figure 4. Time-gated (100−900 μs) PL intensity (as a function of eFluorNC605 concentration) of (a) the Lumi4-Tb donor and (b) the eFluorNC605 acceptor showing efficient FRET donor quenching and acceptor sensitization, which increases until a sAv/eFluorNC605 concentration ratio of approximately one. The PL decay curves of the (c) donor and (d) acceptor show a strongly multiexponential decay behavior caused by FRET from Lumi4-Tb to eFluorNC605 situated at different distances from the QD. Only some representative decay and fit curves are presented. Gray: pure Lumi4-Tb-sAv (The pure Lumi4-Tb luminescence is also visible in the QD detection channel due to spectral crosstalk. This leads to a nonzero time-gated intensity at zero QD concentration in graph b. Such spectral crosstalk can be corrected for multiplexed measurements,[33] but is not necessary for the ratiometric measurement approach we chose for our single donor−acceptor pair experiments); red, 0.06 nM QD; green, 0.1 nM QD; blue, 0.15 nM QD; black, fit curves (for clarity, only a few representative fit curves are shown here).

strongly distance dependent FRET process and the random distribution of Lumi4-Tb-sAv all over the QD surfaces. In prior work we had already demonstrated TR-FRET as a multiplexed molecular ruler for the size and shape analysis of five different types of QDs.[32] The shape analysis of the QDs used within this study by FRET will be further discussed in detail below.

TR-FRET Analysis. Within all FRET experiments the Lumi4-Tb-sAv donor concentration was kept constant at 0.2 nM while the biot-QD concentrations were increased. First, time-gated intensities (100 − 900 μs) were measured simultaneously for the donor and the acceptor on the KRYPTOR fluorescence plate reader system. Afterward complete PL decay curves (from 0 to 8 ms) of the donor and the acceptor were acquired on the EI fluorescence plate reader for selected concentrations in order to perform a time-resolved FRET analysis. The time-gated PL intensity and decay time curves are shown in Figure 4 and 5 for the FRET system Lumi4-Tb-sAv-biot-eFluorNC605 and Lumi4-Tb-sAv-biot-p(DT-SB)605(B). The curves for the other two FRET systems (Lumi4-Tb-sAv-biot-Qdot605 and Lumi4-Tb-sAv-biot-p(DT-SB)605(A)) can be found in the Supporting Information (Figures S2 and S3). For all FRET systems small concentrations of biotinylated QD acceptors (<100 pM) already lead to a significant Lumi4-Tb donor quenching and a very strong QD acceptor sensitization. After a sAv/QD ratio of one is reached (at ca. 0.2 nM QD concentration) these FRET quenching and sensitization processes are saturated because further addition of QDs will not lead to additional FRET-pairs (the concentration of Lumi4-Tb-sAv is constant). Because of several biotins per QD saturation starts already before the complete saturation (flat curve) at Lumi4-Tb-sAv/QD = 1. The number of biotin molecules per QD and the stoichiometry of the FRET systems are discussed in an own section (vide infra). Tb donor quenching is most efficient for p(DT-SB)605, followed by eFluorNC605 and Qdot605. This indicates that the average donor−acceptor distance increases from p(DT-SB)605 to Qdot605 or, in other words, that the QD surface coating thickness increases from p(DT-SB)605 to Qdot605. On the acceptor side Qdot605 and eFluorNC605 show much stronger sensitization than p(DT-SB)605, which can be explained by the differences in PL quantum yields (Table 1).

Time-resolved spectroscopic measurements of lanthanide to QD FRET systems have the large advantage, that the FRET analysis can be performed for both the donor and the acceptor

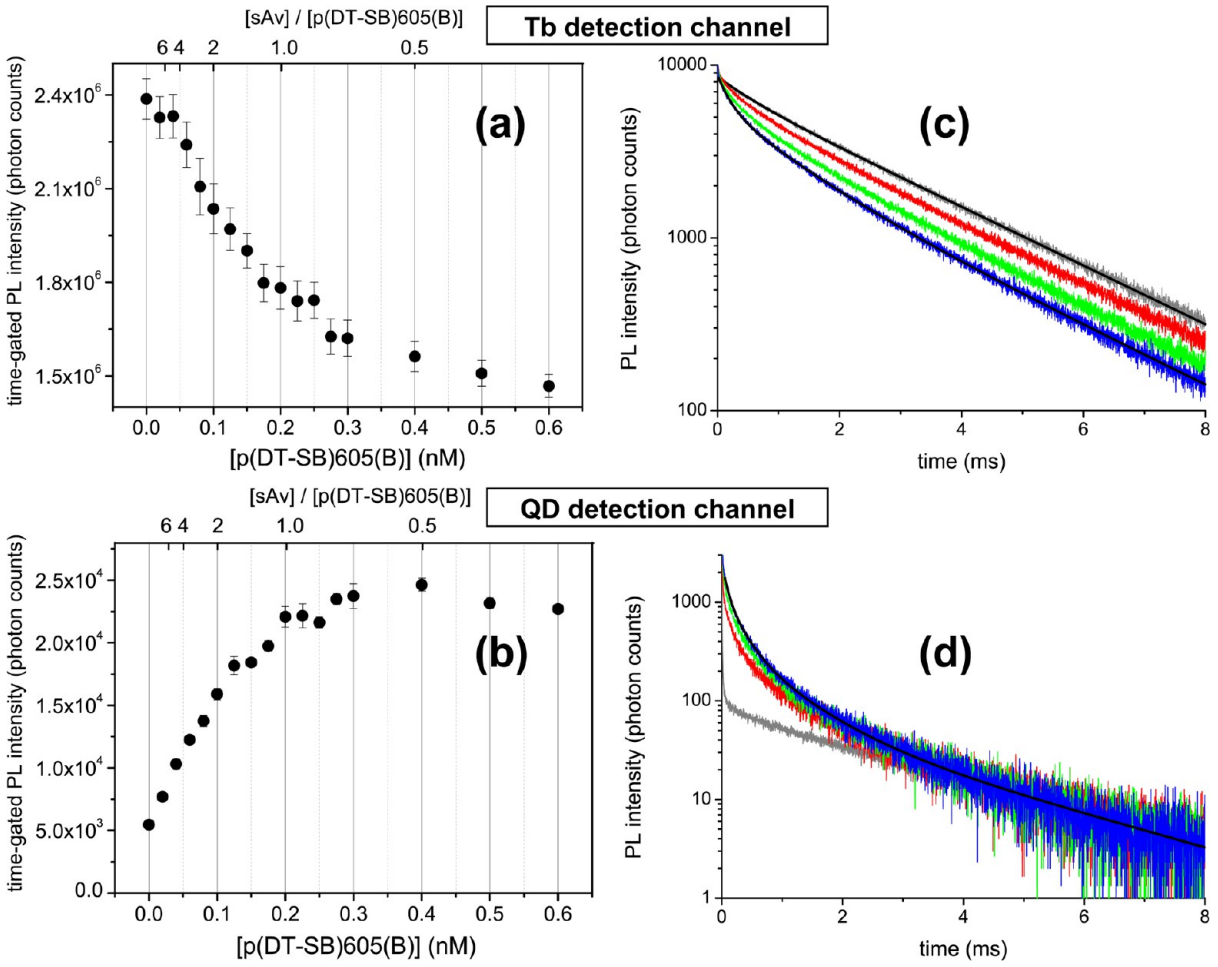

Figure 5. Time-gated (100−900 μs) PL intensity (as a function of p(DT-SB)605(B) concentration) of (a) the Lumi4-Tb donor and (b) the p(DT-SB)605(B) acceptor showing efficient FRET donor quenching and acceptor sensitization, which increases until a sAv/p(DT-SB)605(B) concentration ratio of approximately one. The PL decay curves of the (c) donor and (d) acceptor show a strongly multiexponential decay behavior caused by FRET from Lumi4-Tb to p(DT-SB)605 situated at different distances from the QD. Only some representative decay and fit curves are presented. Gray, pure Lumi4-Tb-sAv (for explanation of Lumi4-Tb emission in the QD detection channel, see caption of Figure 4); red, 0.06 nM QD; green, 0.1 nM QD; blue, 0.15 nM QD; black, fit curves (for clarity only few representative fit curves are shown here).

emission because the FRET-quenched PL decay times can be found in both the FRET-quenched donor and the FRET-sensitized acceptor curves ($\tau_{DA} = \tau_{AD}$ due to the large difference in excited state lifetimes of the Tb-donor and the QD-acceptor).[18] If the same FRET decay times are found for the donor and the acceptor, this will be a strong evidence for energy transfer. Other quenching mechanisms of the donor could lead to different decay behaviors of donor and acceptor. Probably the most important advantage of the time-resolved acceptor analysis is the fact that there is only FRET-sensitized PL because emission from direct QD excitation decays already after some hundreds of nanoseconds and the emission of unquenched donors (which appears as strong background signal in the donor detection channel) does not appear in the acceptor PL. This means that the QD acceptor detection channel is a pure FRET channel. It only requires taking into account spectral crosstalk effects of Tb-donor emission that can still pass through the bandpass filters of the acceptor channel. In the case of the multiexponential decays caused by the Lumi4-Tb to QD distance distribution in our FRET systems an analysis with a small unquenched Tb background PL in the acceptor channel (ca. 20% of the total emission intensity for the Lumi4-Tb-sAv-biot-Qdot605 system) is much more reliable than an analysis with a large unquenched Tb background PL in the donor channel (ca. 80% of the total emission intensity for the same FRET system).

Our PL decay time analysis had two main goals. First, we were interested in the average FRET decay time, which gives access to an average donor−acceptor distance and therefore the average size of the complete QD (including the size of the organic coating around the inorganic QD core/shell system). Second, a determination of different PL decay times and their correlation with the corresponding amplitudes within the exponential decay function could give access to the shape of the different QDs. Within a simplified model we would expect that the very elongated Qdot605 would show at least two average FRET decay times with almost equal amplitude fractions, caused by the two donor−acceptor distances for the minimum and maximum ellipsoid axes of the elongated QD. The other two QDs are more spherical and should therefore show one major FRET decay time (high amplitude fraction) and possibly one minor decay time (due to the fact that they are not perfectly spherical and a minor fraction of a second average donor−acceptor distance should still exist). In particular, we would expect that the ratio of short to long distance decay time amplitude fraction increases with elongation of the QDs (due

dx.doi.org/10.1021/am3030728 | ACS Appl. Mater. Interfaces 2013, 5, 2881−2892

Table 2. Decay Times, FRET Efficiencies, Donor (D)−Acceptor (A) Pair Distances. and Fractions

		Qdot605	eFluorNC605	p(DT-SB)605(A)	p(DT-SB)605(B)
R_0 (nm)		9.1 ± 0.4	7.8 ± 0.3	7.4 ± 0.3	7.4 ± 0.3
$\langle\tau_D\rangle$ (μs)		2310 ± 120	2280 ± 120	2290 ± 120	2270 ± 120
Decay Times (μs) and FRET Efficiencies[a]					
		average			
D	$\langle\tau_{DA}\rangle$	790	890	550	610
	$\langle\eta_{FRET\text{-}DA}\rangle$	0.66	0.61	0.76	0.73
A	$\langle\tau_{AD}\rangle$	630	840	460	540
	$\langle\eta_{FRET\text{-}AD}\rangle$	0.73	0.63	0.80	0.76
		first			
D	τ_{DA1}	270	240	170	200
	$\eta_{FRET\text{-}DA1}$	0.88	0.89	0.93	0.91
A	τ_{AD1}	320	300	160	230
	$\eta_{FRET\text{-}AD1}$	0.86	0.87	0.93	0.90
		second			
D	τ_{DA2}	1110	1110	960	1030
	$\eta_{FRET\text{-}DA2}$	0.52	0.51	0.58	0.54
A	τ_{AD2}	870	1010	600	740
	$\eta_{FRET\text{-}AD2}$	0.63	0.56	0.74	0.67
		third			
A	τ_{AD0}	60	60	30	60
	$\eta_{FRET\text{-}AD0}$	0.97	0.97	0.99	0.97
Donor−Acceptor Distances (in nm) and Fractions[b]					
		average			
D	r_{DA}	8.1	7.2	6.1	6.3
A	r_{AD}	7.7	7.1	5.9	6.1
		first			
D	α_{DA1}	0.40	0.29	0.51	0.52
	r_{DA1}	6.5	5.5	4.9	5.0
A	α_{AD1}	0.40	0.20	0.27	0.32
	r_{AD1}	6.7	5.7	4.8	5.1
		second			
D	α_{DA2}	0.60	0.71	0.49	0.48
	r_{DA2}	9.0	7.7	7.0	7.2
A	α_{AD2}	0.58	0.77	0.69	0.62
	r_{AD2}	8.4	7.5	6.2	6.6
		third			
A	α_{AD0}	0.02	0.03	0.04	0.05
	r_{AD0}	5.0	4.3	3.6	4.1

[a]Errors ± 10%. [b]Errors ± 15%.

to two short axes and one long axis of an elongated ellipsoid), as we have demonstrated before for FRET from Tb donors to QDs with different shapes.[32]

The results of the time-resolved FRET analysis (using eqs 1−11) within both the donor and the acceptor detection channel are summarized in Table 2 (the complete data can be found in the Supporting Information). The data show an excellent match between the results obtained from the donor and the acceptor channel, which gives strong evidence that the energy was efficiently transferred from the donor to the acceptors. Using the QD acceptor decay curves allows for the resolution of an additional decay time (distance) with low emission intensity. This is not possible in the donor channel because of the strong background signal of unquenched Tb-donor emission. Although this "pure" Tb-background was corrected for both channels (cf. eqs 4 and 7) the correction in the donor channel (ca. 80% of the total emission intensity) has much more influence than in the acceptor channel (ca. 20% of the total emission intensity). The strong fraction of long-lived Tb-emission in the donor channel leads to a slight overestimation of the average FRET decay time and distance compared to the acceptor data. Moreover, as amplitude and decay time are correlated (one can compensate for the other) in the mathematical fit procedure,[26] it is more difficult to correctly resolve the donor channel components because the signal to background ratio is lower than in the acceptor channel. Nevertheless, the results from both channels are quite similar, which demonstrates the efficiency of our correction procedures.

Taking advantage of the strong distance dependence of FRET, interesting information about distances and the fractions of donor−acceptor pairs at these distances can be extracted from the data. First of all the average donor−acceptor distance is the longest for Qdot605 and decreases by ca. 1 nm for the eFluorNC605 and an additional 1 nm for the p(DT-SB)605, which clearly shows that the QD coating (separation distance between the photoactive QD core and the biotin molecules on the QD surface) is the largest for Qdot605. As a first

approximation the average donor−acceptor distance can be used as the average radius of the QDs (assuming spherical shape), leading to diameters of ca. (16 ± 3) nm, (14 ± 2) nm, and (12 ± 2) nm for the Qdot605, eFluorNC605, and p(DT-SB)605, respectively. These donor−acceptor distance-based results do not suffer from deviations in size determination because of hydration or elongation of the nanoparticles, which is often the case for dynamic light scattering or size exclusion chromatography.

A closer look at the single distances calculated from the multiexponential fit reveals additional information about the shape of the different QDs. Although the donor and acceptor channel data provide similar information, the acceptor channel should be less error-prone because of the higher signal to background ratio, as already mentioned above. As expected the p(DT-SB)605(A) and p(DT-SB)605(B) show the same results concerning distances and fractions of donor−acceptor pairs at the different distances and they are therefore treated together as p(DT-SB)605 in the following considerations. For the time-resolved FRET analysis these two dots serve rather as another independent control of our fit procedures. Because of the relatively large (no point dipoles) and more or less elongated QDs as well as the random labeling of Lumi4-Tb over the sAv protein all of our investigated FRET systems displayed a donor−acceptor distance distribution. The aim of our time-resolved study was to extract reliable and reproducible information from all the PL decay curves with as few fit parameters as possible. Therefore a triple-exponential fit was applied to the donor PL decays, whereas a quadruple-exponential fit was used for the acceptor PL decays (cf. Experimental Section for details). The determined PL decay times (and distances) can be interpreted as average decay times (and distances) within the overall distribution. All different FRET systems show two main average donor−acceptor distances and one minor average short distance, which can only be resolved within the acceptor channel. The appearance of two main distances shows that none of the QDs is a spherical particle, for which only one major distance component would exist. The different α values in Table 2 represent the fractions of donor−acceptor pairs at the three resolved distances. The amount of donor−acceptor pairs at the shortest distance is almost negligible (below 6% for all FRET systems). However, it is important to include the corresponding decay time in the fits in order to improve the fit result and the resolution of the main two FRET distances. As already mentioned above the fraction of donor−acceptor pairs at the short major distance should increase with elongation of the particle and this is exactly the case for our results. The eFluorNC605 are a mixture of quasi-spherical and tetrahedral QDs (cf. Figure 3 center) with relatively uniform sizes. This is reflected in the relatively small fraction of the short main component (ca. 20% at a 5.7 nm distance). The p(DT-SB)605 are a bit more elongated (Figure 3 right), which results in a relative increase of the short main FRET component (ca. 30% at a 5 nm distance). For the strongly elongated Qdot605 (Figure 3 left) the short main component further increases up to ca. 40% at a 6.7 nm distance. Although it is difficult to determine the exact shape of the nanoparticles with our three main average decay times and their amplitude fractions, these three distances provide very useful information about the QD sizes and shapes under conditions for which they were intended for (a solution phase bioassay at subnanomolar concentrations in our case) instead of "unnatural" conditions such as the analysis on a TEM grid. We believe that our FRET technique is extremely useful to provide this "natural" information, which can be used profitably in combination with the data obtained from TEM, DLS, HPLC or other analytical techniques to complete and/or verify the shape and size information about the QD materials.

Analysis of Unquenched Tb Luminescence and the Number of Biotins per QD. Another interesting aspect of our FRET systems is the remaining unquenched Tb luminescence even at concentrations, for which the QDs are in excess (see the Supporting Information for the complete data). A priori, one would assume that all Lumi4-Tb are quenched (at least partially) once every Lumi4-Tb-sAv has bound to a QD. However, all decay time fits show a significant fraction of unquenched Lumi4-Tb even at QD excess. These fractions are given by the amplitude (α_{DA*3}) of the long unquenched decay time component (τ_{DA3}) divided by the amplitude ($\alpha_{D2} = 0.86$) of this same decay time component for the decay curves of Lumi4-Tb-sAv without biot-QD ($\tau_{D2} = \tau_{DA3}$). This leads to unquenched Lumi4-Tb fractions of 64% for the Qdot605 FRET system, 58% for the eFluorNC605 FRET system, 51% for the p(DT-SB)(A) FRET system and 26% for the p(DT-SB)(B) FRET system. One must take into account that this is not the fraction of unquenched Lumi4-Tb-sAv but of unquenched Lumi4-Tb. Due to the random labeling ratio of 4.2 Lumi4-Tb per sAv some of the Lumi4-Tb complexes are too far away from the QD to be engaged in FRET. This situation is fulfilled for (i) Lumi4-Tb, which is situated on the far end (from the organic QD coating surface) of the sAv (regarding the simplified picture of Scheme 1 this will be approximately 50%), and (ii) Lumi4-Tb-sAv bound to QD coating surface spaces, which are far away from the QD center (because of the nonspherical shape of the QDs, there are closer and further center-to-surface distances). The latter point also explains why the fraction of unquenched Lumi4-Tb is largest for the Qdot605 FRET system (largest and most elongated QD) and decreases for the eFluorNC605 and the p(DT-SB)(A) FRET systems (smaller and less elongated). Another possibility could be a fraction of unreactive (e.g., denatured) Lumi4-Tb-sAv. However, regarding the smallest fraction of unquenched Lumi4-Tb (26%) for the p(DT-SB)(B) FRET system (for which the two long-distance arguments mentioned above are still valid, although less pronounced, see discussion below) and the fact that we used the same Lumi4-Tb-sAv for all FRET systems, the fraction of nonreactive Lumi4-Tb-sAv is rather small (significantly lower than 26%). The large difference in unquenched Lumi4-Tb-sAv for the two similar p(DT-SB)605(A) and (B) systems (only the number of biotins per QD are different) suggests that the higher overall quenching efficiency within the p(DT-SB)605(B) FRET system is caused by the lower number of biotins per QD (see Table 1). The intensity fraction ($\tau_{DA*3}\alpha_{DA*3}$) of the long unquenched Tb luminescence decay component as a function of QD/sAv ratio (see the Supporting Information, Figure S5) shows a linear quenching behavior with increasing amounts of QD, caused by the excess of Lumi4-Tb-sAv. The linear decrease of "pure" Tb emission intensity levels off at QD/sAv ratios below 0.5 and stays at a constant level after 0.5 QD/sAv for Qdot605, eFluorNC605, and p(DT-SB)605(A). This shows that for these QDs several sAv can bind to the QD surface (several biotins per QD) and there is no difference in Tb quenching between several sAv per QD or a single sAv per QD, as long as each sAv is bound to a biotin on a QD surface. The binding situation is different for the p(DT-SB)605(B) FRET system (with ca. 1

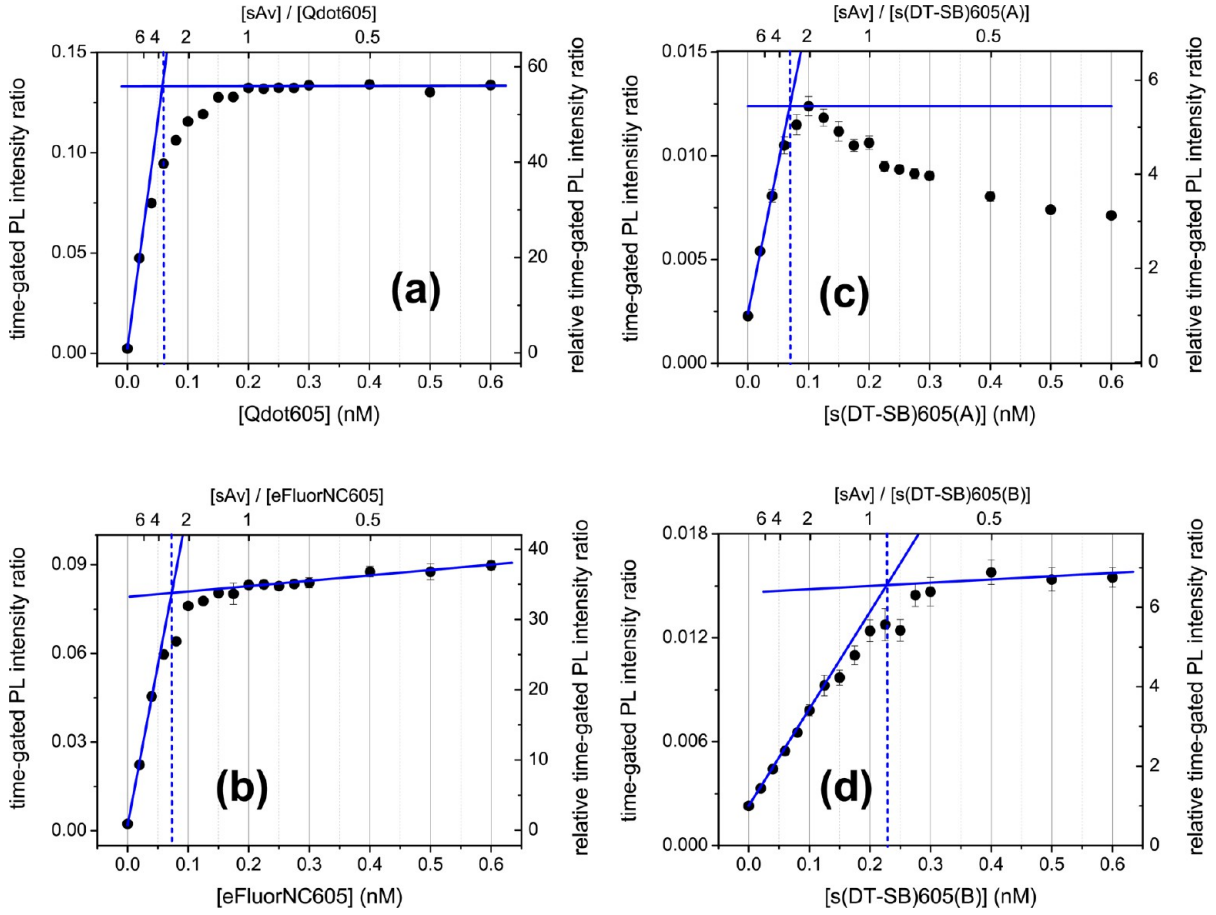

Figure 6. FRET-bioassay calibration curves. Time-gated (100–900 μs) intensity ratios of the FRET systems using Lumi4-Tb as a donor and (a) Qdot605, (b) eFluorNC605, (c) p(DT-SB)605(A), and (d) p(DT-SB)605(B) as acceptors as a function of QD concentration. The Lumi4-Tb-sAv concentration is constant at 0.2 nM within all assays. The intersection point of the blue lines (representing the linear increasing and the saturation parts of the assay curves) is used to determine the biotin molecules on the QD surface (equal to the sAv/QD ratio at that point). Most error bars are smaller than the data points.

biot/QD), for which the attachment of several sAv to one QD is not possible. For p(DT-SB)605(B) it seems that Tb quenching continues even after a 1/1 ratio of QD/sAv. We assume that in this FRET system, the binding of more than one QD per sAv (sAv has four binding sites for biotin) is the preferred system once QD and sAv are in a similar concentration range. This would explain the higher overall quenching efficiency (less unquenched Lumi4-Tb) as there are 4.2 Lumi4-Tb per sAv and the availability of more than one QD for one Lumi4-Tb-sAv leads to the quenching of more Lumi4-Tb per sAv. Figure 6d shows that a complete saturation of FRET-sensitization is reached around 0.5 sAv/p(DT-SB)605-(B), which suggests a formation of a maximum of two p(DT-SB)605(B) per Lumi4-Tb-sAv. For the other three FRET systems FRET-sensitization of QDs is saturated at a concentration of ca. one Lumi4-Tb-sAv per QD and a further addition of biot-QD does not lead to the creation of new FRET pairs (no more free Lumi4-Tb-sAv available). The tangents of the linearly increasing and the saturation parts of the FRET-assay curves were used to calculate the biot/QD ratios, which were 3 to 4 for Qdot605, eFluorNC605 and p(DT-SB)605(A) and ca. 1 for p(DT-SB)605(B). As the sAv/QD axis is not linear a precise determination of the biotin number becomes more difficult the higher the sAv/QD ratio. Nevertheless, we believe that our FRET-based results provide relatively precise results for the biotin labeling ratio (±30%) and thus we conclude that the biot/QD ratio for the Qdot605 is lower than "typically" suggested (5–7 biot/QD) by LifeTechnologies. For p(DT-SB)605(A) the PL intensity ratio curve decreased after saturation, which we attributed to coaggregation of multivalent sAv and biot-QDs, leading to less efficient binding of the Lumi4-Tb-sAv to the biotins on the QD surface when these QDs are in excess. The number of biomolecules per QDs is an important value for many biosensing applications. Our TR-FRET method provides very precise values for the biot/QD ratio measured under physiological conditions at subnanomolar concentrations.

TR-FRET Assays. Our study is based on homogeneous assays, which do not require any separation and washing steps because the FRET signal can be efficiently distinguished from the emission signals of all other components. Therefore, the assay format is very well suited for fast and easily applicable diagnostic tests such as point-of-care diagnostics. A general drawback of point-of-care assays is the lack of sensitivity and thus one of our major goals was the determination of detection limits for our TR-FRET bioassays using the different QD types. The KRYPTOR fluorescence plate reader, a clinical diagnostic plate reader that is commonly used for immunoassays in hospitals and clinical laboratories, is an ideal instrument for comparing sensitivities toward a clinical application. As biotin-streptavidin does not provide an ideal comparison to antibody–antigen immunoassay systems, we used the Eu-TBP/APC

FRET pair (which is used in the commercial BRAHMS-KRYPTOR immunoassays) in the same biotin-streptavidin configuration for comparison. This Eu-TBP-sAv-biot-APC FRET system has an LOD of (24 ± 12) pM.[20] We took advantage of the inherent ratiometric behavior of FRET and used the ratio of the time-gated PL intensities of the QD acceptors (e.g., graphs b in Figures 4 and 5) and the Tb-donor (e.g., graphs a in Figures 4 and 5) in order to achieve a very accurate and highly sensitive quantitative analysis. The time-gated PL ratios as a function of QD concentration for all Tb-to-QD FRET bioassays are presented in Figure 6.

For all four assays the addition of small biot-QD concentrations to Lumi4-Tb-sAv leads to a strong increase of the time-gated PL intensity ratio. This increase is linear until a concentration for which all biotins on the QD surface are bound to one sAv. Higher concentrations lead to a decrease in Lumi4-Tb-sAv per QD and the slope levels off. The limits of detection (LODs) for all assays were calculated as the concentration value for the PL intensity ratio of the sample containing no QDs (zero concentration) plus three times the standard deviation (of 30 measurements). The LOD is dependent on the amount of biotin per QD (more biotin results in a steeper slope), the FRET efficiency and the quantum yield of the QD (the higher these values the steeper the increasing slope of the PL intensity ratio curve). Moreover, the signal-to-noise ratio and reproducibility for the zero concentration sample is important but similar for all FRET systems (as these samples all contain only Lumi4-Tb-sAv). As the biot/QD ratios are not significantly different for the first three QDs the higher quantum yields of Qdot605 and eFluorNC605 are the main aspect that lead to favorable LODs, 0.063 pM and 0.094 pM, respectively, compared to 0.73 pM for p(DT-SB)605(A). The lower biot/QD ratio of p(DT-SB)605(B) leads to an additional increase of the LOD to 2.0 pM. Although these values cannot be transferred as one-to-one to an immunoassay LOD, they are 381-fold, 225-fold, 33-fold and 12-fold lower than the 24 pM LOD for the Eu-TBP/APC "gold standard" FRET system measured in the same biot-sAv configuration. We conclude that all QD systems (commercial and academic) provide very low (pico to subpicomolar) LODs, which means that they are all suitable for highly sensitive biosensing.

CONCLUSIONS

In this TR-FRET study, we have shown that different types of biocompatible QDs (encapsulated and ligand exchanged) can be used for highly sensitive biosensing with low pM to sub-pM detection limits. Our simultaneous TR-FRET analysis of the Lumi4-Tb donor and the QD acceptors allowed us to perform a very precise characterization of the QD materials in terms of shape, size and bioconjugation ratio. We found Qdot605 to be the largest and most elongated QDs with the thickest organic coating around the semiconductor material. Although this thick shell provides the QDs with high stability and brightness, they have the significant drawback of increasing the donor−acceptor distance, which decreases the FRET efficiency. From this point of view the self-synthesized QDs (p(DT-SB)605) show the highest FRET efficiency and thinnest coating. Time-resolved and time-gated analysis also gives close insights into the bioconjugation performance (how many biotins are attached to the QD surface). We could determine biot/QD ratios of ca. 3 to 4 for Qdot605, eFluorNC605 and p(DT-SB)605(A) and ca. 1 for p(DT-SB)605(B). In conclusion we have demonstrated the suitability of all studied QDs for highly sensitive clinical FRET-bioassays. We have performed a very precise and detailed analysis of biocompatible QDs with TR-FRET from Tb-based donor complexes. On the contrary to most of the other analytical technologies (e.g., dynamic light scattering, HPLC and TEM) our FRET method can analyze the biocompatible QDs under physiological conditions at sub-nanomolar concentrations and is therefore highly suited (ideally in combination with the other techniques) to give a more accurate picture of the QD properties at concentrations and conditions in which they are usually applied within fluorescence sensing applications.

ASSOCIATED CONTENT

Supporting Information

(1) Determination of the Förster distances; (2) high-resolution TEM images of Qdot605, eFluorNC605 and p(DT-SB)605; (3) time-gated PL intensities and decays of Lumi4-Tb-sAv-biotQdot605 and of Lumi4-Tb-sAv-biot-p(DT-SB)605(A); (4) control experiments using Lumi4-Tb-sAv and QDs without any biotin on the surface; (5) intensity fraction as a function of p(DT-SB)605(B)/sAv ratio; (6) complete TR-analysis data of the Lumi4-Tb-sAv-biot-Qdot605 FRET system, the Lumi4-Tb-sAv-biot-eFluorNC605 FRET system, the Lumi4-Tb-sAv-biot-p(DT-SB)605(A) FRET system, and the Lumi4-Tb-sAv-biot-p(DT-SB)605(B) FRET system. This material is available free of charge via the Internet at http://pubs.acs.org.

AUTHOR INFORMATION

Corresponding Author

*E-mail: niko.hildebrandt@u-psud.fr.

Notes

The authors declare no competing financial interest.

ACKNOWLEDGMENTS

The authors thank the Ministère de l'enseignement supérieure et de la recherche France (Investissement d'avenir project NanoCTC) and the European Commission (FP7 project NANOGNOSTICS) for financial support.

REFERENCES

(1) Algar, W. R.; Susumu, K.; Delehanty, J. B.; Medintz, I. L. *Anal. Chem.* **2011**, *83*, 8826.
(2) Gill, R.; Zayats, M.; Willner, I. *Angew. Chem., Int. Ed.* **2008**, *47*, 7602.
(3) Jin, Z.; Hildebrandt, N. *Trends Biotechnol.* **2012**, *30*, 394.
(4) Rosenthal, S. J.; Chang, J. C.; Kovtun, O.; McBride, J. R.; Tomlinson, I. D. *Chem. Biol.* **2011**, *18*, 10.
(5) Reiss, P.; Protiere, M.; Li, L. *Small* **2009**, *5*, 154.
(6) Hildebrandt, N. *ACS Nano* **2011**, *5*, 5286.
(7) Hezinger, A. F. E.; Tessmar, J.; Goepferich, A. *Eur. J. Pharm. Biopharm.* **2008**, *68*, 138.
(8) Medintz, I. L.; Uyeda, H. T.; Goldman, E. R.; Mattoussi, H. *Nat. Mater.* **2005**, *4*, 435.
(9) Wild, D. *The Immunoassay Handbook*, 2nd ed.; Elsevier: Amsterdam, 2005.
(10) Bünzli, J.-C. G. *Chem. Rev.* **2010**, *110*, 2729.
(11) Eliseeva, S. V.; Bünzli, J.-C. G. *Chem. Soc. Rev.* **2010**, *39*, 189.
(12) Hemmilä, I.; Mukkala, V. M. *Crit. Rev. Clin. Lab. Sci.* **2001**, *38*, 441.
(13) Selvin, P. R. *Annu. Rev. Biopharm. Biomed.* **2002**, *31*, 275.
(14) Mathis, G. *Clin. Chem.* **1993**, *39*, 1953.
(15) Mathis, G. *J. Biomol. Screen.* **1999**, *4*, 309.
(16) Hemmilä, I. *J. Biomol. Screen.* **1999**, *4*, 303.

(17) Algar, W. R.; Wegner, D.; Huston, A. L.; Blanco-Canosa, J. B.; Stewart, M. H.; Armstrong, A.; Dawson, P. E.; Hildebrandt, N.; Medintz, I. L. *J. Am. Chem. Soc.* **2012**, *134*, 1876.
(18) Charbonnière, L. J.; Hildebrandt, N. *Eur. J. Inorg. Chem.* **2008**, 3241.
(19) Charbonnière, L. J.; Hildebrandt, N.; Ziessel, R. F.; Löhmannsröben, H.-G. *J. Am. Chem. Soc.* **2006**, *128*, 12800.
(20) Geißler, D.; Charbonnière, L. J.; Ziessel, R. F.; Butlin, N. G.; Löhmannsröben, H.-G.; Hildebrandt, N. *Angew. Chem., Int. Ed.* **2010**, *49*, 1396.
(21) Hildebrandt, N.; Charbonnière, L. J.; Beck, M.; Ziessel, R. F.; Löhmannsröben, H. -G. *Angew. Chem., Int. Ed.* **2005**, *44*, 7612.
(22) Xu, J.; Corneillie, T. M.; Moore, E. G.; Law, G.-L.; Butlin, N. G.; Raymond, K. N. *J. Am. Chem. Soc.* **2011**, *133*, 19900.
(23) Li, J. J.; Wang, Y. A.; Guo, W. Z.; Keay, J. C.; Mishima, T. D.; Johnson, M. B.; Peng, X. G. *J. Am. Chem. Soc.* **2003**, *125*, 12567.
(24) Yu, W. W.; Peng, X. G. *Angew. Chem., Int. Ed.* **2002**, *41*, 2368.
(25) Giovanelli, E.; Muro, E.; Sitbon, G.; Hanafi, M.; Pons, T.; Dubertret, B.; Lequeux, N. *Langmuir* **2012**, *28*, 15177.
(26) Lakowicz, J. R. *Principles of Fluorescence Spectroscopy*, 2nd ed.; Kluwer Academic/Plenum: New York, 1999.
(27) Pace, C. N.; Vajdos, F.; Fee, L.; Grimsley, G.; Gray, T. *Protein Sci.* **1995**, *4*, 2411.
(28) Wu, P. G.; Brand, L. *Anal. Biochem.* **1994**, *218*, 1.
(29) Sillen, A.; Engelborghs, Y. *Photochem. Photobiol.* **1998**, *67*, 475.
(30) Liu, W.; Howarth, M.; Greytak, A. B.; Zheng, Y.; Nocera, D. G.; Ting, A. Y.; Bawendi, M. G. *J. Am. Chem. Soc.* **2008**, *130*, 1274.
(31) Uyeda, H. T.; Medintz, I. L.; Jaiswal, J. K.; Simon, S. M.; Mattoussi, H. *J. Am. Chem. Soc.* **2005**, *127*, 3870.
(32) Morgner, F.; Geißler, D.; Stufler, S.; Butlin, N. G.; Löhmannsröben, H.-G.; Hildebrandt, N. *Angew. Chem., Int. Ed.* **2010**, *49*, 7570.
(33) Geißler, D.; Stufler, S.; Löhmannsröben, H.-G.; Hildebrandt, N. *J. Am. Chem. Soc.* **2013**, *135*, 1102.